Measuring errors in single-qubit rotations by pulsed electron paramagnetic resonance

John J. L. Morton,[1,*] Alexei M. Tyryshkin,[2] Arzhang Ardavan,[1,3] Kyriakos Porfyrakis,[1]
S. A. Lyon,[2] and G. Andrew D. Briggs[1]
[1]*Department of Materials, Oxford University, Oxford OX1 3PH, United Kingdom*
[2]*Department of Electrical Engineering, Princeton University, Princeton, New Jersey 08544, USA*
[3]*Clarendon Laboratory, Department of Physics, Oxford University, Oxford OX1 3PU, United Kingdom*
(Received 4 March 2004; revised manuscript received 30 July 2004; published 26 January 2005)

The ability to measure and reduce systematic errors in single-qubit logic gates is crucial when evaluating quantum computing implementations. We describe pulsed electron paramagnetic resonance (EPR) sequences that can be used to measure precisely even small systematic errors in rotations of electron-spin-based qubits. Using these sequences we obtain values for errors in the rotation angle and axis for single-qubit rotations using a commercial EPR spectrometer. We conclude that errors in qubit operations by pulsed EPR are not limiting factors in the implementation of electron-spin-based quantum computers.

DOI: 10.1103/PhysRevA.71.012332 PACS number(s): 03.67.Lx, 76.30.−v, 81.05.Tp

Pulsed magnetic resonance methods have provided a useful playground in which to test different aspects of quantum computation. Single-qubit operations (spin rotations) can be conveniently performed using classical radio frequency (rf) pulses while two-qubit operations can be naturally realized through exchange or dipolar interactions. Exploiting these advantages, the largest-scale quantum computations to date have been demonstrated using nuclear magnetic resonance (NMR) in liquid solution [1,2]. Electron paramagnetic resonance (EPR) offers many parallels with NMR, along with the key advantage that the electron gyromagnetic ratio is of the order of a thousand times larger. Thus pure ground states are experimentally accessible in EPR, avoiding the scalability issues surrounding NMR implementations [3].

For this reason, EPR has become a key element in several solid state quantum information processing (QIP) proposals [4–8]. The practicality of these proposals is critically dependent on the errors that are inherent in pulsed magnetic resonance experiments. In particular, while the decoherence time (T_2) is generally quoted as the ultimate figure of merit for qubit implementations, understanding and minimizing the systematic errors inherent in qubit manipulations is equally important. A number of general approaches to tackling different classes of systematic error in qubit rotations, employing composite rotation sequences, have been proposed [9,10]. However, before these approaches can be exploited practically, it is necessary to characterize (and reduce) the errors that are associated with a single rotation pulse.

There are two principal types of systematic error associated with a single-qubit rotation: rotation angle error and rotation axis error. In magnetic resonance experiments, rotation angle errors arise from an uncertainty in the Rabi oscillation period, associated with uncertainty in the magnitude and duration of the applied rf pulse. On the other hand, rotation axis errors arise from uncertainty in direction of the rf magnetic field in the transverse plane of the rotating frame.

In this paper, we show how multipulse sequences can be applied to measure precisely these two classes of error. These sequences include some originally developed for NMR, as well as a sequence developed specifically for quantifying phase errors. In each case, the sequence amplifies the errors, so that even small errors are detectable. We find that when comparing a commercial EPR spectrometer to an NMR system that has been optimized for high-fidelity qubit operations, rotation angle errors are as good, while phase errors in EPR are worse by as much as an order of magnitude.

The paramagnetic species used here to perform error measurements in pulsed EPR is i-NC_{60} (also known as $N@C_{60}$), consisting of an isolated nitrogen atom in the $^4S_{3/2}$ electronic state incarcerated by a C_{60} fullerene cage. It is an ideal system for these measurements because of its extremely narrow EPR linewidth and long relaxation time in liquid solution [11,12]. T_2 has been measured to be 80 μs at room temperature, rising to 240 μs at 170 K [13].

The production and subsequent purification of i-NC_{60} is described elsewhere [14]. High-purity i-NC_{60} powder was dissolved in CS_2 to a final concentration of $10^{15}/cm^3$, freeze pumped in three cycles to remove oxygen, and finally sealed in a quartz EPR tube. Samples were 0.7–1.4 cm long, and contained approximately 5×10^{13} i-NC_{60} spins. Pulsed EPR measurements were done at 190 K using an X-band Bruker Elexsys580e spectrometer, equipped with a nitrogen-flow cryostat (Janis Research).

i-NC_{60} has an electron spin $S=3/2$ coupled to the ^{14}N nuclear spin $I=1$. The EPR spectrum consists of three lines centered at the electron g factor $g=2.003$ and split by the ^{14}N hyperfine interaction $a=0.56$ mT in CS_2 [15]. However, all the pulsed EPR experiments discussed below were done using the center line in the EPR triplet, corresponding to the ^{14}N nuclear spin projection $M_I=0$. Given the small *isotropic* hyperfine coupling in i-NC_{60}, the transitions with a simultaneous flip of electrons and nuclear spins are largely forbidden and therefore the evolution of electron spin can be treated individually for each nuclear spin manifold. The Bloch sphere is a useful aid to visualize the action of the pulse sequences described below [16]. While this model maps conveniently the magnetization evolution of a single S spin system, the evolution of a coupled $S=3/2$, $I=1$ system

*Electronic address: john.morton@materials.ox.ac.uk

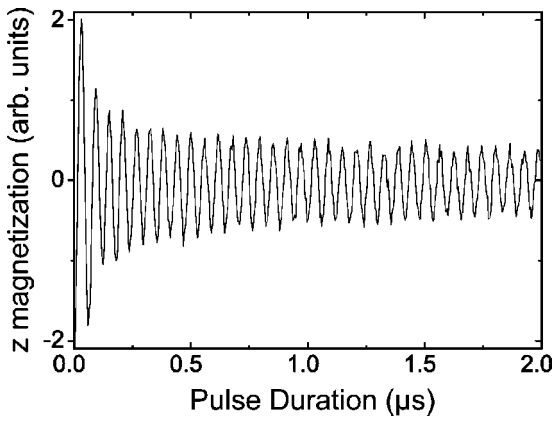

FIG. 1. Rabi oscillations for i-NC_{60} in CS_2 at 190 K.

is harder to visualize. It can be shown that the evolution of the electron spin in the $M_I=0$ manifold is largely unaffected by the presence of the hyperfine coupling and is adequately described by the classical vector model [13].

In an EPR experiment, a qubit rotation is achieved by applying an on-resonance microwave pulse of controlled power and duration. With a pulsed magnetic field strength B_1 and a pulse duration t the rotation angle is

$$\theta = g\mu_B B_1 t/\hbar. \tag{1}$$

Possible off-resonance effects are neglected here because the EPR linewidth for i-NC_{60} is much smaller than the excitation width of the rf pulses used in our experiments. According to Eq. (1), rotation angle errors may arise from either pulse duration errors (which can be assumed uniform throughout the sample), or from errors in the magnitude of B_1 (which can vary across the sample depending on the homogeneity of the EPR cavity mode). The hardware of the EPR spectrometer limits pulse duration to a 2 ns resolution and pulse power to 0.1 dB resolution. These together can contribute of the order of 0.5% to the rotation angle error for a typical 32 ns pulse.

In EPR, measurements are made of the magnetization of the ensemble in the x-y plane, for a static magnetic field applied along z. Hence, a simple measurement of the rotation angle error could be made after a nominal $\pi/2$ rotation, which in practice is $\pi/2+\delta$, where δ is the error. The measured signal is proportional to $\cos(\delta)$. However, this approach is unsatisfactory for two reasons: for a good measurement, a reference (an ideal rotation) is needed with which to compare the imperfect rotation; and the $\cos(\delta)$ term depends on δ only to second order.

Another method involves applying a long rf pulse and observing the Rabi oscillations over a number of periods. The respective experiment for i-NC_{60} is shown in Fig. 1, demonstrating Rabi oscillations whose amplitudes decay at long pulse durations (over 80 oscillations were seen). This decay is caused by inhomogeneity of B_1 fields in the EPR cavity (spins are rotated with slightly different Rabi frequencies and therefore gradually lose coherence), as well as effects such as B_0 field inhomogeneity and the fact that the output power and phase from the microwave amplifier vary

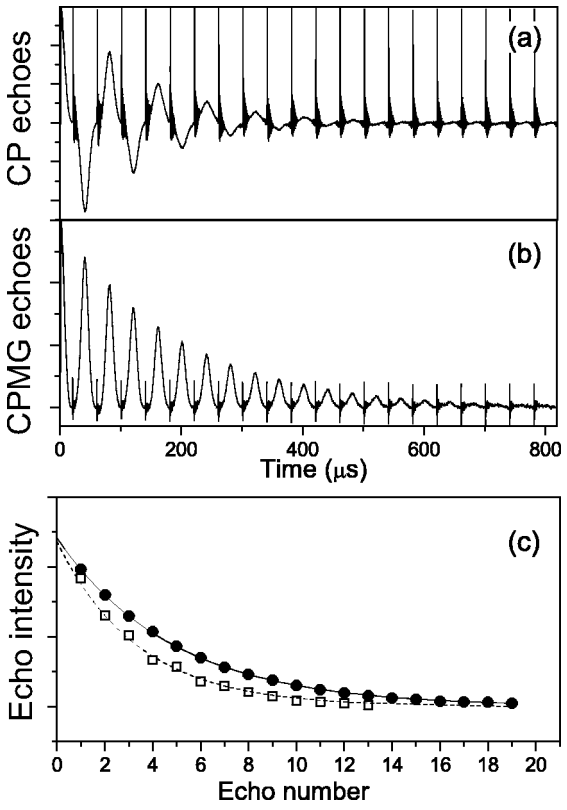

FIG. 2. Comparison of the echo signal decays in (a) the CP and (b) the CPMG pulse sequences. The narrow spikes correspond to the applied π pulses and the echo signals are seen in between. (c) Decay of echo magnitudes for each sequence (CP: empty; CPMG: filled). The solid gray line is a fit to a simple exponential yielding $T_2=190$ μs; the dashed gray line is a fit yielding rotation angle error parameters [17].

at long pulse lengths. In order to distill the rotation angle error from these other effects it is necessary to use more sophisticated methods for error measurement.

A better approach uses sequences of many pulses to compound the error of a single pulse. A suitable sequence, CP (Carr-Purcell [18]), consists of a $\pi/2$ pulse followed by a series of refocusing π pulses, i.e., $\pi/2_x-(\tau-\pi_x-\tau)_n$ in which pulse rotation angle imperfections are additive [19]. The typical exponential decay of the echo is therefore further attenuated by the cumulative rotation angle error, such that the echo amplitude decays with a time constant shorter than T_2. Meiboom and Gill proposed a modification of the CP sequence, termed CPMG (Carr Purcell Meiboom Gill) [20], which compensates for pulse length errors by applying the refocussing π pulses around the y axis.

Figures 2(a) and 2(b) compare the trains of echo signals observed in the CP and CPMG experiments for i-NC_{60}. The decay of the CPMG echo magnitudes is fitted to a simple exponential to obtain the transverse relaxation time T_2. In determining the decay of the echo magnitudes due to rotation angle errors in the CP sequence, we assume the flip angle error follows a Gaussian distribution with mean δ_0 (to account for pulse duration errors) and standard deviation σ_δ (to account for inhomogeneity in the oscillatory magnetic field strength) [17]. From the fit we obtain $\sigma_\delta=18°$ in every 180°

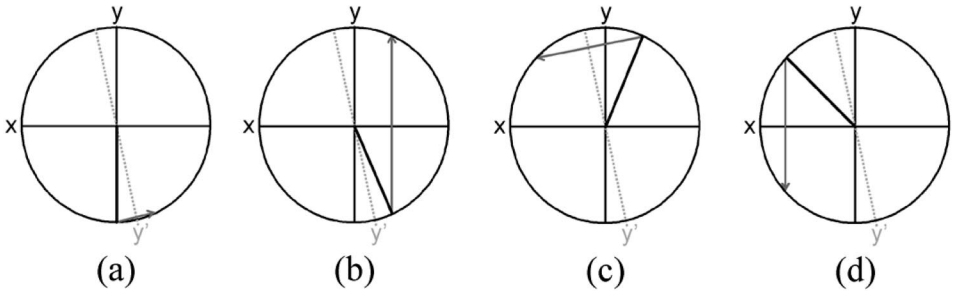

FIG. 3. Evolution of the magnetization vector in the rotating frame during a SPAM experiment. The ideal y and x axes are associated with in-phase and quadrature channels of the quadrature detector, respectively. $\pi/2_x$ and π_x pulses are assumed to be along the x axis; π_y pulses deviate from the ideal y axis by the error angle δ and are oriented along y'. The magnetization vector (bold) is shown (a) immediately after the $\pi/2_x$ pulse, and at times of echo formation after (b) the first π_y pulse, (c) the first π_x pulse, (d) the second π_y pulse. Alternating the refocusing pulses between x and y' in SPAM results in an accumulation of error in the phase of the echo signal.

rotation, or approximately 10%. This figure is consistent with the expected inhomogeneity in the applied B_1 field, and was seen to vary by altering the dimensions of the sample.

Having determined the rotation angle errors, we now turn to the rotation axis errors. The Bruker spectrometer used in this work offers four independent pulse-forming channels, each supplied with uncalibrated analog phase shifter. Our initial goal was to set the microwave phases in two pulse-forming channels to be orthogonal to each other, which is to orient the B_1 field in one channel along the x axis and the other along the y axis. The ideal x and y axes in the rotating frame are defined with respect to the phase of quadrature detection channels, therefore, before perfecting the phase setting of the pulse-forming channels we first examined the orthogonality between the two channels of the quadrature detector. This was done by applying a slightly off-resonance $\pi/2$ pulse and observing the resulting free induction decay (FID) oscillations from each detection channel. A numerical fit revealed an angle of $89.3\pm1°$ between the nominally orthogonal "real" and "imaginary" detection channels.

Traditionally, the phase of a pulse-forming channel is adjusted by applying a simple $\pi/2$ rotation about each channel and observing the FID signal. The inherent imprecision of this approach is not a serious problem in traditional EPR applications in which only a few pulses are applied, but is potentially devastating for the fidelity of a qubit state in a multiple-pulse computation.

In order to measure the orthogonality of the rotation axes in two pulse-forming channels with high precision, we designed a pulse sequence to accumulate phase errors, by analogy with the way that the CP sequence above accumulates flip angle error. This sequence, called sequence for phase-error amplification (SPAM) is given in Eq. (2) and illustrated in Fig. 3,

$$\pi/2_x - (\tau - \pi_y - \tau - \tau - \pi_x - \tau)_n. \qquad (2)$$

After n cycles of this sequence with a phase error δ (i.e., the phase of the π_y pulses is actually $\pi/2+\delta$ with respect to the π_x pulses), the echo vector points along $[\cos(2n\delta), \sin(2n\delta), 0]$. Thus, a nonzero δ in this sequence results in an accumulating "leakage" of the echo amplitude into the orthogonal detection channel, with only a second-order sensitivity to the pulse-length errors described above.

Figure 4(a) shows the echo train obtained in a SPAM sequence for i-NC_{60}. For this experiment, a phase error of approximately 10° between the π_x and π_y pulses was intentionally introduced by observing the FID signals. The measured echo magnitudes for the real and imaginary channels are described by $\cos(2n\delta)$ and $\sin(2n\delta)$, respectively, with an exponential decay envelope $\exp(-4n\tau/T_2)$. n is the number of SPAM cycles (each comprising two refocusing pulses) and T_2 is taken from a CPMG experiment described above. Figure 4(b) shows the echo amplitudes extracted from Fig. 4(a). The fit yields $\delta=(10.3\pm0.5)°$, which is close to the intended phase error. This demonstrates that SPAM is a use-

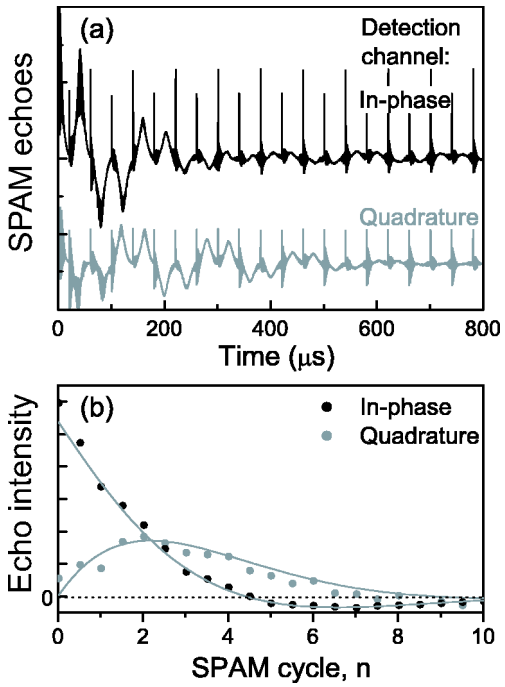

FIG. 4. (a) The echo train from SPAM showing a leakage of signal between the y (in phase: top trace) and x (quadrature: bottom trace) detection channels resulting from phase error between nominal π_x and π_y pulses (traces are offset for clarity). (b) Magnitudes of successive echoes from (a) fitted to functions described in the text yield $\delta=(10.3\pm0.5)°$.

ful way of both measuring the phase error in nominally orthogonal channels, and accurately setting arbitrary phases between channels.

Orthogonality of the π_x and π_y channels was then optimized by traditional procedures (by observing the FID as described above), and a phase error of $\delta=(1.5\pm0.3)°$ was measured from a SPAM sequence. This provides a measure of the phase error typical in conventional pulsed EPR experiments. The fact that it can be measured to a precision of about 0.3° using a SPAM sequence allows us to reduce it substantially further. Careful optimization of the phase error using the SPAM sequence yielded $\delta=(0.3\pm0.1)°$.

In summary, we find that although commercial pulsed EPR spectrometers have not been designed with high precision operations and multipulse sequences in mind, the Bruker machine performs very well. The rotation angle error of about 10% is almost entirely due to the inhomogeneity of the oscillatory magnetic field, and is comparable with those typically observed in NMR [10]. The rotation axis (phase) error of about 0.3° is also comparable with those typically encountered in NMR (though worse than in optimized quantum computing NMR spectrometers).

The most significant strength of the SPAM methodology is that it provides a method of setting relative phases between channels with very high precision. This makes it possible to exploit techniques developed within the context of NMR for applying sequences of pulses at various phases that correct for rotation angle errors [10,21,22]. Such a sequence can reduce a rotation angle error of order ϵ to ϵ^6. Using this approach, our results imply that rotation angle errors can be reduced to the order of 10^{-6}, well within the threshold of 10^{-4} often cited for fault-tolerant quantum computation [23]. This is the subject of a subsequent paper.

We have shown that the technology exists to transfer the quantum information processing methodology that has been developed in the context of NMR to EPR, thereby overcoming the scaling limitations associated with NMR. We conclude that errors in qubit operations do not restrict the viability of an EPR-based quantum computer. Furthermore, we demonstrate the successful application of long pulse sequences (necessary for running quantum algorithms) to an EPR qubit candidate, the *i*-NC_{60} molecule. Finally, we have demonstrated a set of pulse sequences that can be used to amplify and measure precisely the effect of rotation angle and axis errors in any NMR or EPR pulsed magnetic resonance spectrometer.

We would like to thank Wolfgang Harneit's group at the Hahn-Meitner Institute for providing nitrogen-doped fullerenes, and John Dennis at Queen Mary's College, London, Martin Austwick and Gavin Morley for the purification of *i*-NC_{60}. We also thank Jonathan Jones for stimulating and valuable discussions. A Foresight LINK grant *Nanoelectronics at the Quantum Edge*, an EPSRC grant, and the Oxford-Princeton Link fund supported this project. A.A. is supported by the Royal Society. Work at Princeton was supported by the NSF International Office through the Princeton MRSEC Grant No. DMR-0213706 and by the ARO and ARDA under Contract No. DAAD19-02-1-0040.

APPENDIX

In the Carr-Purcell (CP) sequence, $\pi/2_x-(\tau-\pi_x-\tau)_n$, the effect of rotation angle errors is complicated by the dispersion of spins in the *x*-*y* plane due to B_0 field inhomogeneity. For example, those spins pointing along *y* when the refocusing π_x pulse is applied pick up the most error, while those pointing along *x* are unaffected. We assume a uniform distribution of phase, i.e., $\tau \gg T_2^*$, and a Gaussian distribution of rotation angle error with mean δ_0 and standard deviation σ. The echo magnitudes obey the following equation, after the *n*th pulse in the sequence:

$$A_{\mathrm{CP}}(n) = 1 - \sum_{m=1}^{n}\left[a_m + \sum_{k=1}^{m} b_k \exp\left(\frac{-\sigma^2 k^2}{2}\right)\cos(k\delta_0)\right], \tag{A1}$$

$$a_m = \frac{{}^{2m}C_m\,{}^{n+m-1}C_{2m-1}\,{}^{1/2}C_m n(2m-1)}{2m}, \tag{A2}$$

$$b_k = \frac{(-1)^{k2m}\,{}^{2m}C_{m-k}\,{}^{n+m-1}C_{2m-1}\,{}^{1/2}C_m n(2m-1)}{m}. \tag{A3}$$

For $n\sigma<1$, and assuming $\delta_0=0$, this can be approximated to Eq. (A4) below:

$$A_{\mathrm{CP}}(n) = \exp\left(\frac{-\sigma^2 n^2}{4}\right). \tag{A4}$$

To fit the CP decay we use $A_{\mathrm{CP}}(n)\exp(-t/T_2)$, with T_2 taken from the CPMG fit.

[1] M. A. Nielsen and I. L. Chuang, *Quantum Computation and Quantum Information* (Cambridge University Press, Cambridge, 2000).
[2] D. G. Cory, A. F. Fahmy, and T. F. Havel, Proc. Natl. Acad. Sci. U.S.A. **94**, 1634 (1997).
[3] W. S. Warren, Science **277**, 1688 (1997).
[4] B. E. Kane, Nature (London) **393**, 133 (1998).
[5] G. Burkard, H. A. Engel, and D. Loss, Fortschr. Phys. **48**, 965 (2000).
[6] W. Harneit, Phys. Rev. A **65**, 032322 (2002).
[7] A. Ardavan, M. Austwick, S. C. Benjamin, G. A. D. Briggs, T. J. S. Dennis, A. Ferguson, D. G. Hasko, M. Kanai, A. N. Khlobystov, B. W. Lovett, *et al.*, Philos. Trans. R. Soc. London, Ser. A **361**, 1473 (2003).
[8] S. A. Lyon (http://arXiv.org/abs/cond-mat/0301581).
[9] M. H. Levitt, Prog. Nucl. Magn. Reson. Spectrosc. **18**, 61 (1986).
[10] H. K. Cummins, G. Llewellyn, and J. A. Jones, Phys. Rev. A

67, 042308 (2003).
[11] E. Dietel, A. Hirsch, B. Pietzak, M. Waiblinger, K. Lips, A. Weidinger, A. Gruss, and K. P. Dinse, J. Am. Chem. Soc. **121**, 2432 (1999).
[12] C. Knapp, K. P. Dinse, B. Pietzak, M. Waiblinger, and A. Weidinger, Chem. Phys. Lett. **272**, 433 (1997).
[13] A. M. Tyryshkin, J. J. L. Morton, A. Ardavan, K. Porfyrakis, S. A. Lyon, and G. A. D. Briggs (unpublished).
[14] M. Kanai, K. Porfyrakis, G. A. D. Briggs, and T. J. S. Dennis, Chem. Commun. (Cambridge) **2**, 210 (2004).
[15] T. Almeida-Murphy, T. Pawlik, A. Weidinger, M. Hohne, R. Alcala, and J. M. Spaeth, Phys. Rev. Lett. **77**, 1075 (1996).
[16] A. Schweiger and G. Jeschke, *Principles of Pulse Electron Paramagnetic Resonance* (Oxford University Press, New York, 2001).
[17] See the Appendix.
[18] H. Y. Carr and E. M. Purcell, Phys. Rev. **94**, 630 (1954).
[19] R. Freeman, *Spin Choreography: Basic Steps in High Resolution NMR* (University Science Books, Sausalito, CA., 1997).
[20] S. Meiboom and D. Gill, Rev. Sci. Instrum. **29**, 688 (1958).
[21] S. Wimperis, J. Magn. Reson. **109**, 221 (1994).
[22] K. Brown, A. Harrow, and I. Chuang, Phys. Rev. A **70**, 052318 (2004).
[23] A. M. Steane, Phys. Rev. A **68**, 042322 (2003).